Characterizing fluvial systems at basin scale by fuzzy signatures of hydromorphological drivers in data scarce environments

R. Schmitt [a,c,*], S. Bizzi [b,c], A. Castelletti [c]

[a] Institute of Environmental Engineering, ETH Zurich, CH-8093 Zurich, Switzerland
[b] European Commission, Joint Research Centre, Institute for Environment and Sustainability, Via E. Fermi, 2749, I-21027 Ispra, VA, Italy
[c] Department of Electronics, Information, and Bioengineering, Politecnico di Milano, P.za L. da Vinci, 32, I-20133 Milano, Italy

Article history:
Received 24 August 2013
Received in revised form 23 February 2014
Accepted 27 February 2014
Available online 12 March 2014

1. Introduction

Rivers are highly dynamic and hierarchic landscape elements, where local and regional forms and processes depend on specific signatures of physical drivers interacting over different spatio-temporal scales along a downstream continuum (Frissell et al., 1986; Petts and Amoros, 1996; Knighton, 1998). In this context, river hydromorphology (HYMO) defines geomorphological and hydrological signatures of the fluvial system and their spatio-temporal interference and variation (Newson and Large, 2006; Vaughan et al., 2009). In turn, HYMO processes affect local ecological functioning, infrastructure and water resource availability, and quality (Simon and Rinaldi, 2006; Vaughan and Ormerod, 2010; Boon et al., 2012). The accurate, process-based assessment of hydromorphological dynamics in a river system is thus key to support river basin planning and management (Brierley and Fryirs, 2008; Sear et al., 2010). Unfortunately, despite the recent success of HYMO assessments for informing river managers (Brierley et al., 2002), systematic, process-based assessments of large river systems are still scarce in most developed countries (Newson and Large, 2006) and basically absent in least developed or emerging economies (Lall, 2011). In these contexts, where increasing anthropogenic pressure on the environment directly translates into rapid transformation of the fluvial system, such accurate comprehension of river geomorphology is a key aspect for long-term sustainability (Wohl, 2006; Brierley and Fryirs, 2008; Gupta et al., 2012). Recent paradigms in fluvial system science perceive physical appearance and ecological functioning of rivers as a result of continuous change and local discontinuity in HYMO drivers (Gurnell and Petts, 2011; Carbonneau et al., 2012) and the transverse interaction of rivers with surrounding landscape elements (Whigham and Young, 2001; Richards et al., 2002; Vaughan et al., 2009). When regarding fluvial systems as hierarchical, with smaller units nested into larger ones, each individual unit is subject to a location specific, unique signature of HYMO drivers that is controlled by higher-hierarchical levels (Frissell et al., 1986) and that distinguishes it from adjacent up- and downstream units. The emergence of morphological features—their spatial extension, dynamics and resilience to change—results, accordingly, from the distinctive local signature of HYMO drivers. Assessing HYMO dynamics thus requires consideration of local processes, understanding of the interference of larger hierarchical units with local phenomena, and an assessment of the spatio-temporal scale of these interferences.

* Corresponding author at: Department of Electronics, Information, and Bioengineering, Politecnico di Milano, P.za L. da Vinci, 32, I-20133 Milano, Italy. Tel.: +39 223 993 579.
E-mail address: RafaelJan.Schmitt@polimi.it (R. Schmitt).

Classification, as the process of ordering objects into a number of classes based on certain class-defining attributes, is a commonly applied approach to extract features from such complex systems. With regard to river channels, numerous attempts have been undertaken to subdivide the rivers' downstream continuum into smaller, discrete sections based on single or multiple criteria (e.g., Kondolf et al., 2003; Buffington and Montgomery, 2013). For fluvial systems, a large variety of specific classification schemes has been developed for various geographic contexts and spatial scales (Kondolf et al., 2003; Thorp et al., 2006; Brierley and Fryirs, 2008; Buffington and Montgomery, 2013). Amongst these, a main subdivision is between approaches that identify geomorphic processes and those providing a mere characterization of morphological forms (Simon et al., 2007). Often, the last-mentioned approaches focus on surveying physical habitats within river systems as, for instance, the River Habitat Survey (Raven et al., 1998) and similar frameworks worldwide (Barbour et al., 1999; Parsons et al., 2003). These methods have been extensively applied on large scales as they are based on well-established monitoring activities and simple classification criteria (Somerville and Pruitt, 2004). Yet, they are of limited operational value as they fail to characterize underlying HYMO processes (Newson and Large, 2006; Simon et al., 2007) and thus do not permit to predict adaptation to changed conditions. In contrast, process-related classification schemes, based on detailed site assessments of local HYMO drivers, processes, and forms, have been implemented to successfully support river management needs (Brierley et al., 2002; Brierley and Fryirs, 2008; Sear et al., 2010). The resulting spatio-temporally distributed understanding of riverine processes provides a structured framework to inform managers and support decision-making, and constitutes the backbone of a classification framework to collect and store additional (e.g. ecological) information (Brierley et al., 2002; Sear et al., 2010). Despite their high value for river management, process-based classifications are still scarcely available for a number of reasons (Buffington and Montgomery, 2013). The necessity for a detailed assessment of local conditions as well as of the overarching setting requires resource-demanding field work with direct in situ observations and data collection, e.g., hydrological, geological, and historical information. Physical access, domain expertise, and availability of data are often limited, particularly in developing countries because of limited transport infrastructure, conflict situations, or hindered information exchange between abutting nations in large fluvial basins. Here, remote sensing platforms provide easily accessible, spatio-temporally distributed data and present a great potential to change the physical assessment of river hydromorphology (Marcus and Fonstad, 2008; Fonstad and Marcus, 2010; Buffington and Montgomery, 2013). Remote sensing data sets have been widely used to characterize morphological processes: physical drivers, e.g., in terms of slope and/or stream power, have been successfully applied to identify breakpoints in morphological processes (Reinfelds et al., 2004; Carbonneau et al., 2012; Vocal Ferencevic and Ashmore, 2012) and to disaggregate fluvial systems by means of advanced statistical techniques (Leviandier et al., 2012). Nevertheless, identification of river reaches characterized by similar forces, processes, and forms from distributed multidimensional HYMO data sets is a recent research challenge that largely has yet to be addressed (Alber and Piégay, 2011; Bizzi and Lerner, 2012). Even though remote sensing data are available for wide regions, real implementations of spatially extended river classification schemes are scarce or absent—and yet more specific frameworks need to be developed—if the potential of remotely sense information is to be fully exploited in river science and management (Carbonneau and Piégay, 2012). Moreover, advanced process-based river classification schemes do so far exclusively consider crisp divisions between individual river reaches (Brierley and Fryirs, 2008; Rinaldi et al., 2013). This approach contradicts the common notion of rivers being characterized by a downstream continuum (Vannote et al., 1980) as well as by local and abrupt discontinuities (Poole, 2002). It is also not compatible with observations of morphological appearance of fluvial channels not being related to clear thresholds in physical drivers (Ferguson, 1987). To address the need for consistent, globally applicable and process-related fluvial classification and management tools, we propose a new approach towards the challenges posed by the large-scale assessments of fluvial systems. We develop a framework to store and structure big and multidimensional HYMO data sets including commonly available remote sensing information. From this large, multivariate data sets we derive characteristic combinations of HYMO drivers by means of a machine-learning based classification mechanisms. By integrating a fuzzy classifier, the framework is able to distinguish continuous from abrupt downstream change in HYMO drivers, to identify breakpoints and to quantify rates of downstream change. This approach is demonstrated for the Red River Basin in Northern Vietnam and China. Here, strong morphologic changes in the river system were observed, that impact e.g. water resource use in the delta region. In contrast, very limited information is so far available regarding the upstream hydro-morphologic conditions in the basin. For this large basin, we provide evidence how a multi-scale framework, derived on the basin scale from global data sets and generalizations based on few available field data, furthers the understanding and supports modelling from the basin scale to reach level processes.

2. Case study

The Red River Basin was selected as a study area for the application and validation of the proposed methodology. Located between 20°00′ and 25°30′ N and between 100°00′ and 107°10′ E on the SE Asian mainland (Fig. 1), it covers an area of around 169,000 km^2 (Thanh et al., 2004; Dang et al., 2010), of which 50.3% is located in Vietnam, 48.8% in China, and 0.9% in Laos (Le et al., 2007; Dang et al., 2010). The western part of the basin is divided into the three subbasins of the Thao, Da, and Lo that all, after originating from the China's Yunan Mountain range, discharge in the west–east direction (Fig. 1). The three subbasins are distinctly different in their meteorological as well as their tectonic forcing, resulting in subbasin-specific patterns of topography, sediment production and land use (Table 1).

After the confluence of the 3 tributaries 50 km upstream of Vietnam's capital city Hanoi, the newly formed main stream of the Red River enters a delta plain that extends westward until the Gulf of Tonkin. As hydropower constitutes the largest single contribution to the rapid growing national energy demand of Vietnam, four major multipurpose reservoirs have been constructed in the Lo and the Da River subbasins (Fig. 1) over the last 40 years. Besides hydropower production, all reservoirs serve to protect the downstream urban centers from flooding and provide interseasonal water storage for downstream paddy rice production (Castelletti et al., 2012) at the same time impact hydrologic and sedimentologic changes, for example incision processes, induced by upstream impoundments, river morphology and endanger a variety of human activities from gravity fed irrigation to river infrastructure. The high diversity within a single basin, the multiple and partially conflicting water uses, its vast extent, the presented socioeconomic challenges, and the impact of current water management practices on local and large-scale HYMO urge for the development of effective and sustainable basinwide water management strategies. The complete lack of any structured HYMO information makes the Red River basin a challenging testing ground for the proposed methodology.

3. Methods and tools

The methodology we propose for the creation of the spatially distributed HYMO data set can be divided into four interconnected steps (Fig. 2). The data sets available for this study are detailed in Table 1. In step one, the fluvial network was derived from a digital elevation model (DEM) and dissected into sections of equal length (1000 m). Topographic information in terms of Strahler order (O_s), floodplain width (W_{FP}), drainage area (A_D) and slope (S) was subsequently derived from the DEM along the extracted network (Section 3.1). In step 2, some

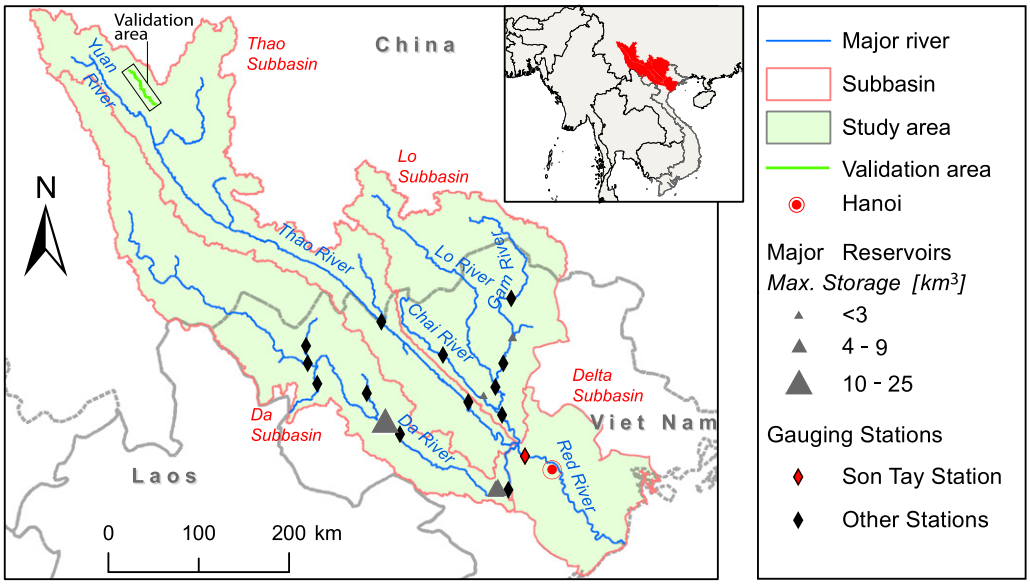

Fig. 1. Overview over the study area indicating the major reservoirs, the 14 gauging stations used in this study, and the tributary of the Thao River used for validation of the methodology.

physical drivers and geomorphic information were obtained as point measurements, e.g., local discharge; derived from gauging stations; or active channel width (W_{Ac}); measured from satellite imagery. Based on these point data and topographic information, the effective discharge (Q_{Eff}) was computed at the gauging stations using a stochastic modelling approach to determine local sediment transport (Section 3.2). Subsequently (step 3), point data were upscaled to the entire network and from the resulting distributed data set, channel confinement ratio (C) and specific stream power (ω) were calculated (Section 3.3). In the classification step (step 4), using an unsupervised two-stage clustering approach consisting of a neural network coupled to a fuzzy clustering algorithm, a low number of characteristic signatures were derived from the high-dimensional input data set. Subsequently, each reach within the river network was assigned a specific HYMO signature based on the local values of six HYMO drivers (O_S, S, $Q_{1.5}$, Q_{Eff}, C, ω) (Section 3.4).

3.1. Spatial analysis

The central part of spatially distributed morphological analysis (Fig. 2, step 1) was based on the Aster V2 GDEM, a globally available digital elevation model (DEM) with 30-m horizontal resolution (Fujisada et al., 2012). The stream network was delineated following the procedure outlined by O'Callaghan and Mark (1984). The delineated stream network provided primarily a template along which geomorphic drivers were measured from the DEM. As a representation of the actual fluvial network, the derived stream lines also served for the spatial referencing of other attributes and to assign the results of the fuzzy classifier to specific river sections (Alber and Piégay, 2011). The *Strahler order* (Strahler, 1957) was calculated for the digital network as representation of the network's topology in terms of hierarchy and branching properties. The original raster network was vectorized and split at each confluence node. In between nodes, stream lines were split at regular intervals of 1000 m. The resulting river segments constituted the basic unit of analysis and will be further referred to as 'reaches'. The *bedslope* of the channels was determined along each reach using the elevation difference between start- and end-nodes. Where topographic information was lost from the original DEM during the filling process (Rieger, 1993, 1998), slope was interpolated from the elevation of adjacent up/downstream sections.

Regarding *floodplain width*, various methodologies have been proposed to discriminate the valley bottom, i.e. the fluvial corridor including floodplain and active channel from adjacent, hill-slopes using DEMs (e.g., Alber and Piégay, 2011 and the references therein). From the proposed methods, based either on the analysis of valley bottom shape or on the topographic analysis defining the floodplain as the area inundated during a certain, morphologically relevant flood stage, the latter methodology was selected. This was due to the relatively low resolution of the available DEM through which detailed topographic information regarding valley bottom shape was lost during the filling process. Several authors proposed to scale the applied flood stage with certain local channel properties (e.g., Nardi et al., 2006), but in this case study, a fixed flood stage (10 m) was assumed, due to the lack of otherwise required, hydro-geomorphic data. Similar criteria were adopted by (Alber and Piégay, 2011) for a similar application. The *floodplain width*, W_{Fp}, was subsequently measured by casting regularly spaced transects from the stream-lines. For each reach, three transects in the end, mid and start points were casted. Given the available DEM resolution, the active channel was not distinguishable from the floodplain and could not be derived directly from the DEM. Therefore, the *active channel width* W_{Ac} was manually sampled from optical satellite imagery at 25 randomly selected points for streams of each Strahler order ($n_{tot} = 200$). In general, the active channel could be distinguished well from the floodplain by the absence of vegetation. Given the

Table 1
Key meteorologic, topographic and resulting land use characteristics for the 3 upstream basins of the Red River basin (Rangin et al., 1995; Van Maren, 2005; Le et al., 2007; Trinh et al., 2012).

Sub basin	Area [km^2]	Max. elevation [m]	Mean slope [%]	Mean precipitation [mm a^{-1}]	Dominant land use
Thao	57.150	6740	33	1904	Forest (54.2%)
Da	51.285	3145	37	1884	Forest (74.4%)
Lo	34.559	3076	20	1874	Mixed crops (58.6%)

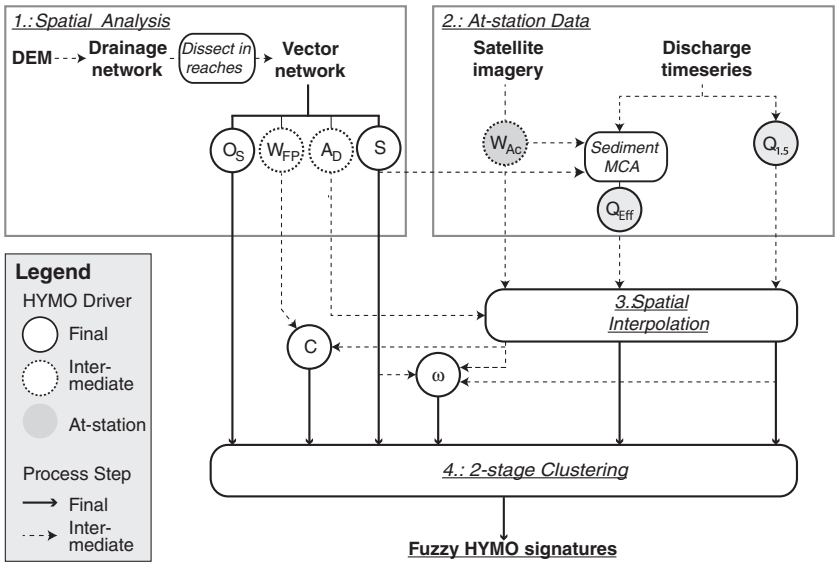

Fig. 2. Flow chart of the HYMO framework to derive spatially distributed HYMO drivers (O_S: Strahler order; S: slope; $Q_{1.5}$: discharge with 1.5 yr return period; Q_{Eff}: effective discharge; C: confinement; ω: stream power; A_D: drainage area; W_{Ac}: active channel width; W_{FP}: floodplain width) to derive a process-correlated classification based on unsupervised classification techniques.

prevalently high available image resolution (see Table 2) and the measured median channel width (125 m) accuracy of measurements is considered sufficiently high. These point data were generalized according to the procedure outlined in Section 3.3. While slope and discharge determine the main driving forces in terms of fluvial morphology, the channel *confinement ratio* can be seen as an indicator of the ability of the channel to adjust laterally to the driving forces and as a major control of local river morphology (Brierley et al., 2002). Channel confinement ratio C was calculated as the ratio of local lateral floodplain extent W_{Fp} and active channel width W_{Ac} (Nicoll and Hickin, 2010).

3.2. At-station data: analyzing hydrological and sediment transport data

The second step of the methodology (Fig. 2) concerned the analysis of daily discharge time series of an average length of 39 years recorded at 14 gauging stations in the basin (Fig. 1 and Table 2). Certain statistical properties of discharge time series, namely $Q_{1.5}$ and the *effective discharge*, Q_{Eff}, were extracted following the original notion by Frissell et al. (1986), where different discharge processes influence different spatio-temporal scales of channel-forming processes. To identify differences in the discharge forming processes between different gauging stations, the discharge with a return period of 1.5 years was extracted for each station. Without in-situ measurements available, this return period was selected as a consistent indicator for a channel forming discharge which, in specific contexts, represents bankfull discharge (Knighton, 1998; Garcia, 2008). Following Wolman and Miller (1960), the effective discharge was computed integrating discharge and sediment transport regime into a common indicator (Garcia, 2008). Accordingly,

$$Q_{Eff} = \max_{Q}(f(Q), C_t(Q)) \tag{1}$$

where $f(Q)$ denotes the empirical probability density function of discharge Q, and $C_t(Q)$ the sediment transport as a function of discharge. The effective discharge identifies the discharge with the highest cumulative sediment transport capacity. As empirical sediment transport data were available in an aggregated form (sediment rating curves) and for one station (Son Tay, see Fig. 1) only, a numerical procedure was developed to estimate sediment transport from the local hydraulic conditions. A Monte-Carlo Simulation was implemented based on the empirical Meyer-Peter–Müller (MPM) equation (Meyer-Peter and Müller, 1948), which is a commonly used and well-tested transport load predictor in comparative sediment transport studies (Wong and Parker, 2006, and the references therein). The MPM equation relates the sediment transport $C_t(Q)$ to local hydraulic conditions as follows:

$$C_t(Q) = \frac{8}{g}\frac{\rho_p}{\rho_p - \rho_l}\sqrt{\frac{1}{\rho_p}}\left[\rho_p\ g\ S\ R_h(Q, S, W_{Ac}, k_{St}(d50)) - \tau_{crit}\left(\rho_p - \rho_l\right)\ g\ d_{50}\right]^{\frac{3}{2}} \tag{2}$$

where g is the gravitational acceleration, ρ_p,ρ_l are the particle and liquid density, respectively, S is the bedslope, and τ_{crit} is the critical shear stress for incipient sediment motion. $R_h(Q,S,W_{Ac},k_{St}(d50))$ is the hydraulic

Table 2
Overview of the data sets used in this study.

Distributed data	Spatial resolution	Accuracy
Optical imagery (obtained via Google Earth (Google Inc., 2013))		
Digital Globe Quickbird	Up to 0.65-m (Carbonneau and Piégay, 2012)	No data
CNES Spot Image	Up to 2.5-m (Carbonneau and Piégay, 2012)	No data
Topographic data		
Aster V2 GDEM	30-m	±17-m (Fujisada et al., 2012)
Point data	**Temporal resolution**	**Time series length**
Discharge data (14 stations)	1 day	12–60 yrs (μ = 39 yrs)
Sediment rating curves at Son Tay station (Dang et al., 2010)	30/24 yrs (1960–1989, 1985–2008)	60 yrs

radius as a function of discharge Q, bedslope S, active-channel width A_C and the Manning–Strickler coefficient k_{St}, itself a function of the median grain size diameter d_{50}. This calculation of channel hydraulics $R_h(Q)$ based on the Strickler equation was performed assuming a rectangular channel cross section (Negrel et al., 2011), with W_{Ac} derived from satellite imagery for the respective station. Eq. (2) was repeatedly run at a sampling step of 50 $m^3\ s^{-1}$ between the minimum recorded Q and $Q_{1.5}$ for each gauging station. For each step, 200 individual realizations of Eq. (2) were evaluated based on random values for four relevant hydraulic parameters (d_{50},W_{Ac},S,k_{St},τ_{crit}) generated based on the distribution parameters detailed in Table 3.

Sediment grain size was assumed to have a uniform distribution between a minimum and a maximum grain size in dependence of the Strahler order at the respective station (Table 4).

A first-order power law function was fitted to the resulting sample of $C_t - Q$ pairs (Asselman, 2000). The obtained synthetic sediment rating curve $C_t^{synth}(Q)$ was used in place of $C_t(Q)$ in Eq. (1) to estimate the effective discharge at each gauging station.

Results of the simulation closely matched empirical rating curves derived by Dang et al. (2010) (Fig. 3) for Son Tay station (see Fig. 1) for the period before (blue line) and after (green line) the construction of a major reservoir (Hoa Binh reservoir) in the Da catchment. Calculated values (black dots) for C_t and fitted, synthetic rating curve $C_t^{synth}(Q)$ (red line) matched closely the observations in the period before the construction of the reservoir. The sediment transport was overestimated in comparison to the current situation: the calculation approach considered only sediment transport capacity, but the strongly altered sediment supply due to upstream impoundments and other anthropogenic activities in the RRB (Le et al., 2007; Dang et al., 2010), which is in line with regional (Lu and Siew, 2006; Yang et al., 2006; Saito et al., 2007; Dai and Lu, in press) and global observations (Walling and Fang, 2003; Syvitski et al., 2009) could not be considered in this calculation.

Notably, given the fact that we only included medium resolution remote sensing data, the match between measured and simulated sediment transport was satisfactory. The proposed methodology could be greatly enriched by empiric sediment data, where available. Nevertheless, in the scope of a comparative river classification, this sediment model represented a consistent indicator of potential sediment transport in the function of local hydraulic conditions.

3.3. Spatial interpolation

As a third step of the methodology (Fig. 2), at-station data were upscaled to the entire river network by regression techniques. $Q_{1.5}$ and Q_{Eff} were scaled using a power law regression on the drainage area (Knighton, 1999). Two different regression approaches were tested to generalize the discharge. First, a regression including all stations was implemented. Second, separate regressions for each subbasin were calculated. The quality of the models was evaluated in terms of both, correlation coefficient (R^2) and accordance with reported exponent values, indicating that Q increases under-proportionally with A_d (Knighton, 1998). Results of this analysis pointed out the difference between the two indicators Q_{Eff} and $Q_{1.5}$ and justified the use of both as metrics in the data set (Fig. 4). For Q_{eff}, the basin wide regression did not result in the highest R^2, but subbasin wise regressions for Lo and Thao subbasins did not result in adequate $Q - A_D$ relations (Fig. 4, left panel). In contrast, for $Q_{1.5}$ the subbasin wise regressions clearly outperformed the basin wise regression approach (Fig. 4, right panel).

In these terms, $Q_{1.5}$, which was based on a discharge with constant return period, characterized reaches in terms of the discharge regime related to their geographic position in the subbasins. In contrast, Q_{Eff} characterized the local balance between driving (slope, discharge) and resisting (sediment size) forces. These aspects were rather controlled by local conditions than by geographic positioning of reaches in a distinct subbasin.

To scale W_{Ac}, Huang and Nanson (2002) proposed a second-order power law regression, relating it with S and $Q_{1.5}$ and, thus, to the drainage area through the above-described power regression linking flow and drainage area. Finally, the specific stream power ω was computed as

$$\omega = \frac{g\rho_l QS}{W_{Ac}}. \tag{3}$$

Several studies pointed out the ability of remote-sensing derived ω to identify breakpoints in physical processes and forms along a river continuum (Reinfelds et al., 2004; Orr et al., 2008; Vocal Ferencevic and Ashmore, 2012; Bizzi and Lerner, 2013), being a low-level indicator for the locally available energy (Hickin and Nanson, 1984; Nanson and Hickin, 1986).

3.4. Classification

To derive an HYMO classification of the river network under study, a two stage clustering approach was applied to the data set generated in the previous steps (step 4, Fig. 2). First, a neural network was applied to preclassify reaches based on their HYMO drivers and to visualize the high dimensional correlations between the HYMO drivers. Second, a fuzzy clustering algorithm was used to identify a manageable number of characteristic driver signatures from the neurons and, accordingly, to derive an HYMO classification of the entire fluvial network. The derived data set of HYMO drivers contained the six hydro-morphological parameters (O_S, S, $Q_{1.5}$, Q_{Eff}, C, and ω) for the entire river network (28,887 reaches). As a first classification step, a self-organizing map (SOM, Kohonen, 1990) was derived from the original data set. The SOM is an unsupervised learning approach based on neural networks to map high-dimensional data sets on low-dimensional displays. The approach was already applied successfully to the multivariate classification of single river sections (Bizzi and Lerner, 2012), wherein also the concrete application and relevant parameters for applying SOMs to river channels are detailed. In a second step, a fuzzy clustering algorithm (FCM, fuzzy c-means clustering, Bezdek, 1981) was applied to the SOM to delineate broader groups of neurons representing reaches with similar hydromorphological characteristics. This is a major advantage over existing, crisp classifications (Bizzi and Lerner, 2012) that *i*) did not distinguish abrupt change from continuous adjustments and *ii*) discarded all information of the reaches similarity to other classes by assigning a reach to a single class. In contrast, FCM stores, for each observation, the distance to all cluster centers in a metric referred to as membership function. Each identified cluster center represents a characteristic HYMO signature. The local values of the membership function reproduced the degree of similarity of an individual reach to all HYMO

Table 3
Input value parameter distributions for the 5 input variables of the sediment MCA at each station *i*.

Input parameters	Input statistical distribution	Explanation
d_{50}	$d_{50min,i} < d_{50,i} < d_{50max,i}$; d_{50min}, $d_{50max} = f(OS,i)$	Uniform distribution with min. and max. grain size depending on Strahler order
W_{AC}	$\mu = W_{AC,i}$, $\sigma = W_{AC,i} * 0.05$	$W_{AC,i}$ measured from Quickbird/Spot imagery
S	$\mu = S_i$, $\sigma = S_i * 0.05$	S_i derived from Aster V2 GDEM
k_{St}	$\mu = k_{St} = f(d_{50})$, $\sigma = 0.05 * k_{ST}(d_{50,i})$	k_{St} calculated from median grain size
τ_{crit}	$\mu = 0.047$, $\sigma = 0.05 * \tau_{crit}$	Derivation from critical shear stress due to local form effects

Table 4
Grain size distribution as a function of the Strahler order for the Monte Carlo Simulation of sediment transport.

Parameter	Strahler order			
	3	4–5	6	7–8
Grain type	Cobbles to medium gravel	Medium gravel to very coarse sand	Very coarse to coarse sand	Coarse to very fine sand
Min. grain size [mm]	8	1.5	0.75	0.05
Max. grain size [mm]	250	8	1.5	0.75

signatures. Continuous change in the HYMO signature was represented by a gradual downstream change in the membership functions of the river reaches. Since its development in the 1970s, the fuzzy *c*-means algorithm was widely applied to identify patterns in large data sets based on the iterative minimization of a cost function of the form

$$C = \sum_{k=1}^{n}\sum_{i=1}^{c}\mu_{ik}^{m}||x_k - v_i||^2 \quad (4)$$

where n is the number of data points, c is the number of clusters, x_k is the kth data point and v_i is a cluster center. μ_{ik}^{m} is the membership value of data point k to the cluster i weighted by m, where m controls the fuzziness of the individual clusters. According to Chiu (1994), a value of $m = 2$ was implemented in this study. The membership value was defined as distance metric to the cluster centers in the form of

$$\mu_{ik} = \frac{1}{\sum_{j=1}^{c}\left(\frac{||x_k - v_i||}{||x_k - v_j||}\right)^{2/m-1}}. \quad (5)$$

Based on an a priori definition of the number of clusters and an initial guess for the position of the cluster centers v_i, the FCM algorithm converges to a solution for v_i that represents a local minimum or a saddle point of the cost function (Bezdek et al., 1987). To overcome the need for a user-defined, a priori definition of clusters, Chiu (1994) proposed a methodology to derive the number of cluster centers purely data driven. It evaluates the potential of each data point to form a cluster center by means of an additional performance metric. Iteratively, data points with the highest performance value are selected as a cluster center. Commonly, the procedure is stopped as soon as the incremental decrease in performance drops below a certain threshold ϵ based on the empirical evaluation by a domain expert on the final number of classes to be obtained (e.g., Yager and Fileu, 1993). In this study we used an evolution of this approach for a purely data-driven identification of cluster centers. Instead of a crisp ϵ, a range of ϵ and an additional performance measure were implemented (Chiu, 1994). For $\overline{\epsilon} > \epsilon > \underline{\epsilon}$ (with $\overline{\epsilon} = 0.5$ and $\underline{\epsilon} = 0.15$) an additional measure quantified if the data-point had sufficient potential for representing a new cluster center by comparing its overall potential to its distance to already identified cluster centers. In our case study, the number of identified cluster centers represented the number of characteristic HYMO signatures. Each reach could be assigned to a dominant HYMO signature — i.e., the characteristic HYMO signature to which it had the highest membership function value. In addition, the value of the membership function of all other HYMO signatures represented their local relevance for the distinct reach.

4. Results

The fluvial network for the Red River basin contained 21,042 km of rivers, divided into 28,887 reaches with an average length of 728.45 m. For each the values of the six physical HYMO drivers were derived. Based on these driver values, each reach was mapped onto a SOM map unit (Fig. 5, panel A).

As the position of a distinct reach was the same along the plots for the six HYMO drivers, the comparison of the maps allowed us to visually assess the distribution of reaches amongst the SOM neurons. The color

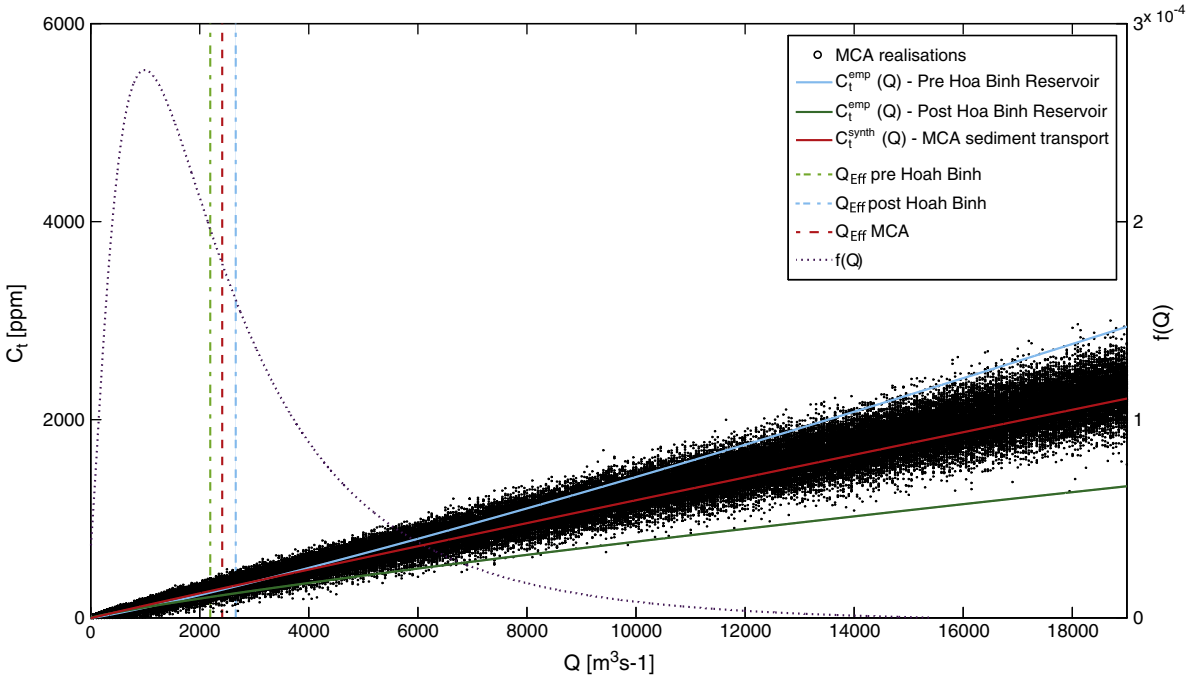

Fig. 3. Comparison of the empirical sediment rating curves from Dang et al. (2010) (blue and green) and the synthetic sediment rating curve calculated using results from the MCA approach (red). Vertical lines visualize the derived Q_{Eff} values for Son Tay gauging station.

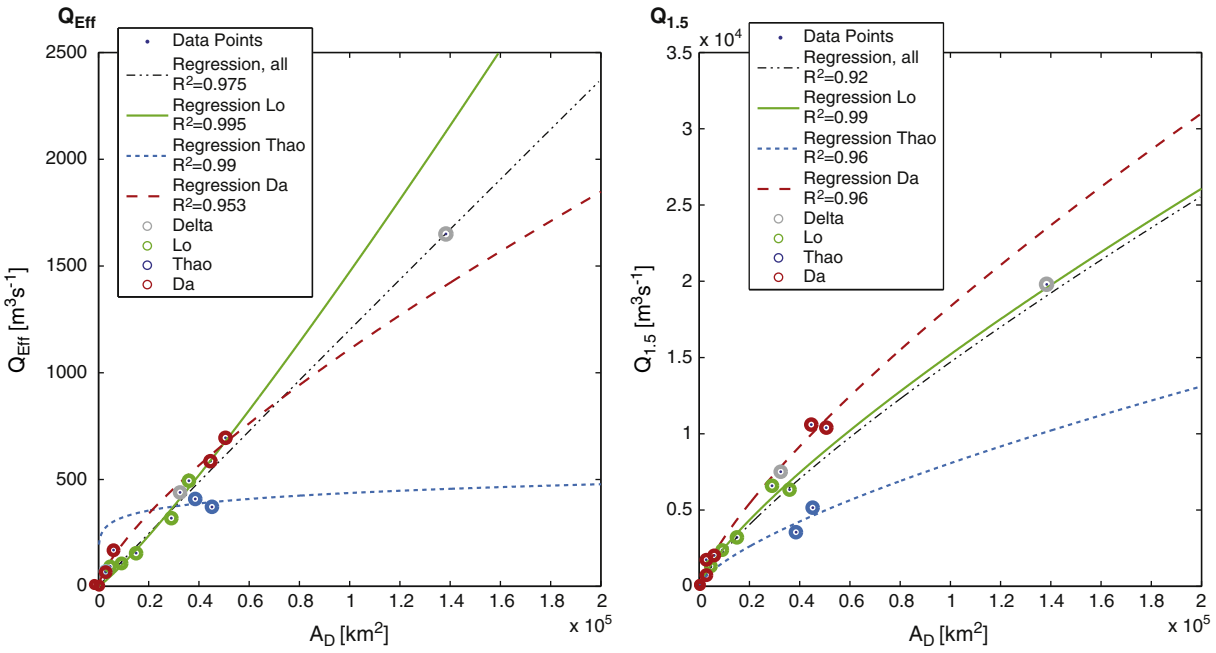

Fig. 4. Comparison of subbasin-wise regression approaches versus regression approaches including the entire basin to estimate effective (left panel) and bankfull (right panel) discharges.

code indicates the average value of the HYMO drivers for the reaches assigned to a neuron. Reaches with very large discharge were placed to the upper right corner of the SOM, which was correlated to high values for Strahler order O_S in contrast to very low values for slope S

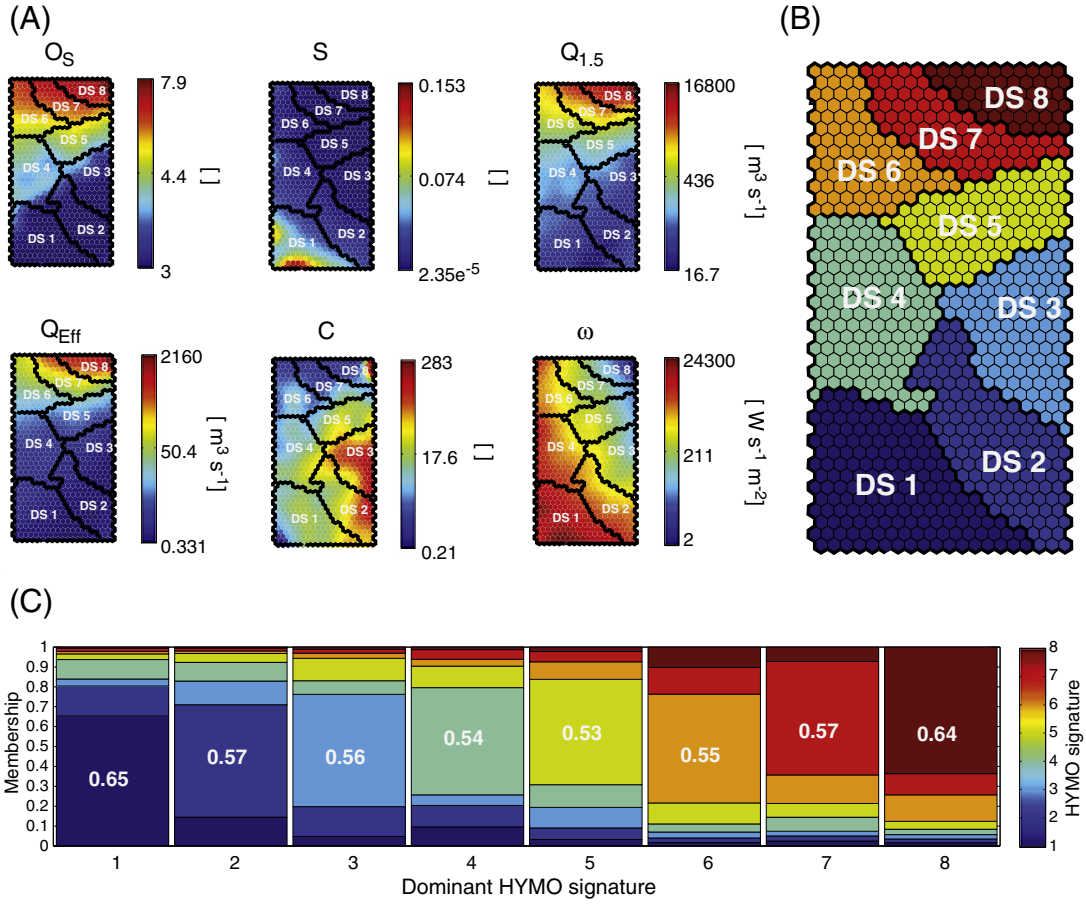

Fig. 5. Self organizing maps (SOM) for six HYMO drivers (A). Boundaries identifying the dominant HYMO signatures were derived by the fuzzy clustering algorithm (B). As a result of the fuzzy classification, the members of each dominant signature are identified by a characteristic interference of HYMO signatures (C).

and stream power ω. In contrast, reaches with very high S were located at the lower left corner of the SOM. This area corresponded to small reaches with very low O_S, Q_{Eff}, and $Q_{1.5}$. Peaks in ω corresponded to peaks in S but, in contrast to S, the distribution of values over the SOM was relatively homogeneous. With ω being a function of $Q_{1.5}$, it also showed a gradient from the lower left to the upper right corner. Whereas $Q_{1.5}$ showed basically the same gradient as O_S, Q_{Eff} showed a different pattern. The well defined area of diverging Q_{eff} and $Q_{1.5}$ indicated a subset of reaches, for which the two different generalization approaches resulted in the most significant divergence. Concretely, Q_{eff} of reaches in this group is relatively small in comparison to $Q_{1.5}$. Whereas all aforementioned physical drivers could be related to certain internal gradients along the river network, the distribution of channel confinement C amongst the SOM neurons revealed that confinement was not significantly correlated to any of the other physical drivers. Accordingly, the confinement was indicating specific local reach characteristics that depended strongly on external forcing like lithology, geology and physiography and not on internal gradients along the river network (Notebaert and Piégay, 2013).

Based on the SOMs, eight characteristic HYMO driver features – or signatures – were identified by the FCM algorithm (Table 5) which are further referred to as characteristic HYMO signatures 1–8 (HS 1–8).

Each HYMO signature represented a distinctive configuration in the multidimensional space of the six HYMO drivers analyzed. The HYMO signatures characterized the reach domain in terms of its driving and resisting forces within which fluvial processes and forms can develop. Marking the position of the different HYMO signatures on the self organizing map (Fig. 5B) enabled the comparison of key differences between the characteristic HYMO signatures in terms of physical drivers and to assign them a broad location in terms of up- or downstream position in the entire river network (Table 2). Fig. 5C clarifies the advantages of using fuzzy clustering to assess the interference of characteristic HYMO signatures. Each reach was characterized by a dominant signature (DS), i.e., the HYMO signature to which it had the highest degree of belonging. Reaches of DS 1, for example, were in average by 0.65 characterized by HS 1. Fig. 5C also quantifies the 'similarities' amongst different HYMO signatures: e.g., reaches of DS 3 are more similar to HS 2 (blue) than to HS 4 (turquoise) or 5 (green).

5. Implementation and application

Transferring the resulting classification back into a GIS, the spatial pattern of HYMO signatures was available for further numerical analysis or expert based morphologic evaluation for the entire river network — from the basin scale down to individual reaches.

We demonstrated its application first on the basin scale differentiating spatial sub-units (subbasins) in terms of their distinct HYMO signature. Spatial distribution of HYMO signatures as result of topographic and hydro-meteorological subbasin characteristics was visualized and compared for the subbasins' fluvial networks. Next, analysis of HYMO signatures focused on an extended section of a single river and investigated morphological forms resulting from location-specific interferences of morphological signatures. To conclude the analysis, HYMO signatures were applied to the temporal rather than the spatial domain and correlated to local rates of morphological change in a numerical modelling scheme.

5.1. Characterizing river network composition at subbasin scale

Analyzing and comparing the aggregated HYMO signatures of the fluvial networks allowed for an effective assessment of (dis)similarities in driving forces between different spatial entities. Here, we focused on topographic entities (subbasins). Topographic and hydro-climatic differences strongly impacted the composition of the subbasin fluvial network (Fig. 7). With regard to headwater or smaller reach types (see Table 5) of DS 1–3 there was a clear distinction between the Lo and the Thao/Da subbasins. Steep, channel head reaches of DS 1 and 2 constituted a significant lower percentage of the fluvial network in the Lo subbasin, in accordance, channel heads were formed here by reaches of DS 3 characterized by low ω and high C (Fig. 5). Similar patterns occurred for DS 4 and 5, respectively 6 and 7 where DS 5 and 7, characterized by a low ω and high C are over-represented in the Lo subbasin. In general patterns of inter-subbasin (dis)similarities, Thao and Da subbasins displayed a relative similarity for cumulative network composition mainly for DS 1 and 2 while Da and Lo became increasingly similar in this regard for DS 3–8.

Fig. 6 exemplifies the visualization of results for the Da and the Lo subbasins. Such an assessment can indicate the spatial distribution of DS (Fig. 6A and B) and the downstream progression of reach types in the fluvial network as well as the pattern of any characteristic HS (Fig. 6C & D exemplifies the visualization for HS 4). A visual assessment clarified that reaches with a high degree of belonging (>0.75) to HS 4 displayed a distinctively different distribution between the Lo and the Da subbasins: whereas being relatively homogeneously distributed within the latter these reaches were concentrated in few separated pockets in the former. A simplified representation of the dominant HYMO signatures of the entire fluvial network in the RRB is made available as .kmz-file (color code in accordance with Fig. 6A & B) for further, interactive assessment.

These considerations demonstrated that the HYMO data set could be aggregated for the drainage networks of larger spatial units. Accordingly, it provided specific HYMO characteristics of such extended units. The derived, classification framework cannot only be aggregated on the large scale but can also be applied to provide a consistent metric for comparing HYMO characteristics on smaller scales for more detailed analysis.

5.2. Analyzing local river signatures

On even smaller scales, for individual river sections, the validity of the classification framework in terms of its correlation to local morphology and HYMO processes needed to be verified. Therefore, we analyzed in more detail the HYMO signatures obtained for a specific river in the Thao subbasin (Fig. 1). Given the lack of field measurements, high resolution satellite images were used as a reference (see Table 2). Key question in this context was whether the methodology, based on the

Table 5
The eight characteristic signatures in terms of HYMO drivers (++: very high, +: high, o: medium, −: low, – –: very low) and their function in the fluvial system.

Characteristic signature	HYMO drivers						Description
	O_S	S	$Q_{1.5}$	Q_{Eff}	c	ω	
1	– –	++	– –	– –	+	++	Dominant in channel heads of mountainous and steep reaches.
2	– –	+	– –	– –	++	++	Dominant mainly in midland channel heads.
3	−	+	– –	– –	++	o	Dominant in head to mid-valley, lowland reaches.
4	o	+	o	−	+	++	Dominant in mid-valley, mountainous reaches.
5	o	o	o	o	o	o	Dominant in mid-valley, lowland reaches.
6	+	−	+	o	−	+	Dominant in mid-valley, lowland reaches transition to major streams
7	++	−	++	++	– –	o	Dominant in lowland reaches of large rivers.
8	++	−	++	++	– –	– –	Dominant in lowland reaches of major rivers.

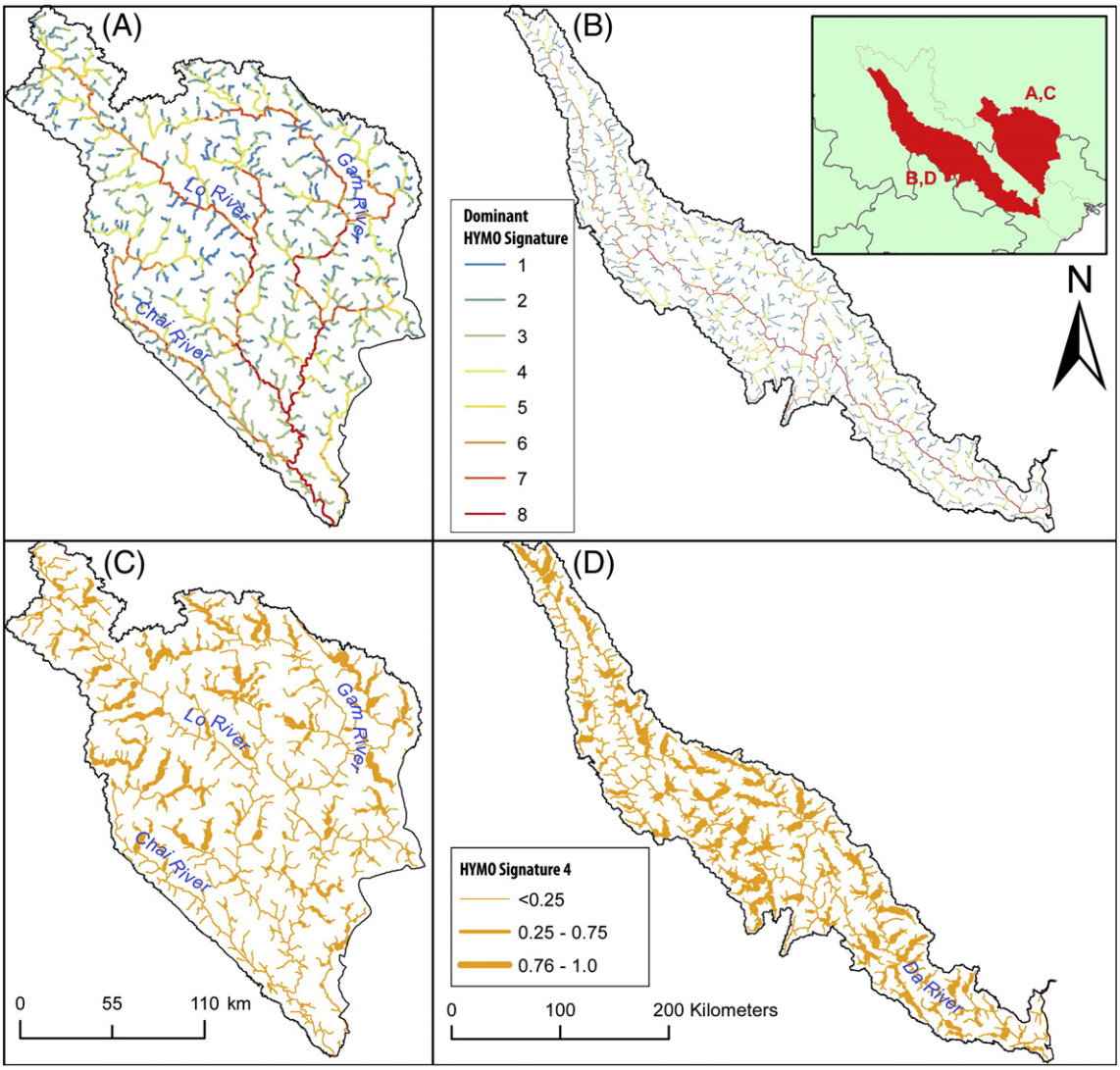

Fig. 6. Transferring results of the classification back into a GIS allows us to visualize the spatial distribution of HYMO signatures e.g., for distinct subbasins (A & C: Lo subbasin, B & D: Da subbasin). Panels in the top row (A and B) visualize the spatial distribution of dominant signatures. Panels in the bottom row (C and D) exemplify the visualization of the MSF to a specific HYMO signature (here: HYMO signature 4).

derivation of physical drivers from medium-resolution remote sensing data, correctly identified breakpoints in local morphology, which were, in turn, related to location specific, nontrivial signatures in driving forces. For a thorough interpretation, relevant geo-spatial data can be assessed as .kmz-file via Elsevier's online GIS services. The file included contains (a) the dominant signatures of the entire Red River Basin and (b) all eight, fuzzy HYMO signatures for the catchment (1942 km^2, 398 reaches) encompassing the validation case study.

Seventeen changes in the dominant HYMO signature were identified along the river under study dissecting it into 18 sections (Fig. 8, 1–18). The average section length L_{sect} was 3.95 km or ~4 reaches. In general terms, the river under study displayed a decrease in HS 4 and, at the same time, a constant increase in HS 6, which represented a continuous, downstream transition amongst these two HYMO signatures. Within this smooth transition, four abrupt changes in the dominant signature could be detected (Fig. 8, I–IV) — namely most often changes from HS 4 to HS 5 (I–III) or, farther downstream, towards HS 6 (IV).

Continuous changes in physical drivers translated into the patterns of HS signatures. For example, a continuous increase in slope and a decrease in confinement were observed between sections 17 and 18. These gradients translated into a continuous increase in HS 6 and a decrease in HS 5. Also within single sections, complex changes in physical drivers were coherently associated with similar patterns in the HYMO signatures. For instance, all reaches within section 5 belonged DS 4; but nevertheless, the local HYMO signatures displayed significant downstream change related to specific, local interference of physical drivers, e.g., in S, ω, and C. The developed HYMO framework was then able to derive a classification that identified local multivariate signatures of physical drivers and included them into a fuzzy framework that allowed us to distinguish local breakpoints in processes from continuous downstream change. Two examples are now discussed in more detail to demonstrate that the classification related to changes in morphological forms and processes detected on high resolution images available.

Referring to Fig. 8, moving from section 3 to section 4 located a drop in S and ω that coincided with a continuous decrease in C. This change in physical drivers was reflected in the HYMO signatures as a decrease in value of HS 4 and an increase in HS 5. For section 4, HS 5 became dominant. In section 5, the values of S and ω returned to values close to those observed for section 3. Also, confinement increased continuously downstream. Reaches in section 3 were characterized by a higher sinuosity and signs of major lateral migration as well as no sustained vegetation in the active channel (compare zoom boxes). Reaches in section 4

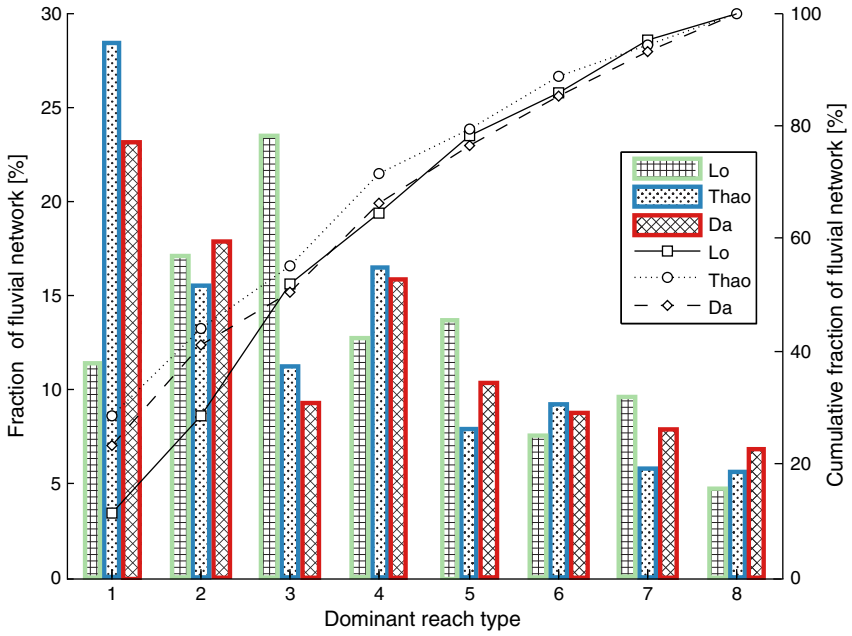

Fig. 7. Subbasin-wise aggregated HYMO signatures.

(HS 5) displayed clearly less signs of lateral migration, a reduced active channel width, and pockets of vegetation/agriculture on the banks of the active channel indicated a reduced lateral mobility. These observations are in line with the measured decrease in energy and confinement for this section. Entering in section 5, S, ω, and C returned to values similar to section 3. These abrupt changes were attributed to a changing valley profile, which became narrower for section 4, limiting the river's capacity to create meanders and enhanced channel conveyance (compare zoom boxes). For Fig. 8, example 2 (sections 7, 8, 9), an initial abrupt decrease in slope and ω coincided with a local peak in confinement. Within section 8, C, S and ω presented opposite trends with decreasing C and increasing S and ω. The abrupt change in physical drivers induced a strong shift in the classification from HS 4 to HS 5 (breakpoint III). For downstream reaches of section 8, membership to HS 4 and 6 increased continuously until HS 4 became again dominant in section 9. Between sections 7 and 8 the most notable distinction was observed in terms of active channel width. After the confluence with a small tributary, the active channel widened abruptly. This development reached its peak in a large pocket of alluvial deposits that also showed signs of continuous lateral migration and channel bifurcation (Fig. 8, EX2, zoom box), indicating low lateral channel stability. This feature was located upstream of five bedrock spurs, which induce a strong local increase in sinuosity. Reduced transport capacity within the sinuous sections created the wide and relatively flat active channel upstream owed to the deposition of excess sediment. Accordingly, as the excess sediment was readily deposited upstream, the sinuous reaches themselves showed a continuous change back to the channel pattern observed for section 7. Breakpoint III was explained accordingly as local deviation from the average up/downstream slope because of a sediment imbalance induced by a tributary and coinciding with downstream external geological forcing on channel sinuosity. In this case, disturbance of the sediment balance leads to an abrupt initial change followed by a continuous re-adaptation to the new supply of water and sediment within the geologic context present. The longitudinal scale over which the processes took place was reflected in the abrupt, respectively continuous, changes in the membership functions.

The above findings indicated that the HYMO signatures conveyed relevant information in terms of morphologic appearance and dynamics and identify morphologic breakpoints. The HYMO signatures coherently supported the visual interpretation of morphological forms as a result of non-trivial, multidimensional interference of HYMO drivers. Last, a numerical model experiment was designed to evaluate if the derived classification was significantly correlated to the occurrence of in channel morphological elements and to temporal morphological dynamics.

5.3. Predicting processes and forms

Morphological features and dynamics were derived from high resolution satellite imagery for the above-mentioned river section. A novel model type was developed to predict these features from the fuzzy HYMO signatures aggregated over the variable length sections defined above. As performance test, this model approach was benchmarked against models making use of fixed aggregation length and/or locally measured physical drivers. Three sets of high resolution satellite imagery were available for the case study via Google Earth (Google Inc., 2013) for the years 2001, 2006 and 2012. Three morphological variables, (*i*) thalweg migration; (*ii*) pool frequency; and (*iii*) accumulated pool length were derived from the satellite imagery by expert-based delineation. The thalweg was defined as center line of the water surface during low flow conditions. The lateral migration of thalweg between image capture dates was measured in terms of Euclidian distance from the previous position of the thalweg. Pools were mapped from the 2012 image set only as change between image capture dates was not significant. Pools could be readily distinguished from ripples or runs given the available image resolution. Pool frequency was defined as number of pools per kilometer, whereas the accumulated pool length was defined as sum of pool surface length per kilometer of stream.

As described above, reaches could be further aggregated into sections with a single dominant HYMO signature. As stated above, each section contained a variable number of reaches based on the results of the classification. Values of physical drivers, HYMO signatures and morphological variables were derived for the sections as the arithmetic mean over participating reaches. As comparison, two alternative approaches were included into the validation: one approach used no aggregation and worked accordingly on the reach scale ($L_{sect} = 1$). The second approach was based on an aggregation of reaches into sections

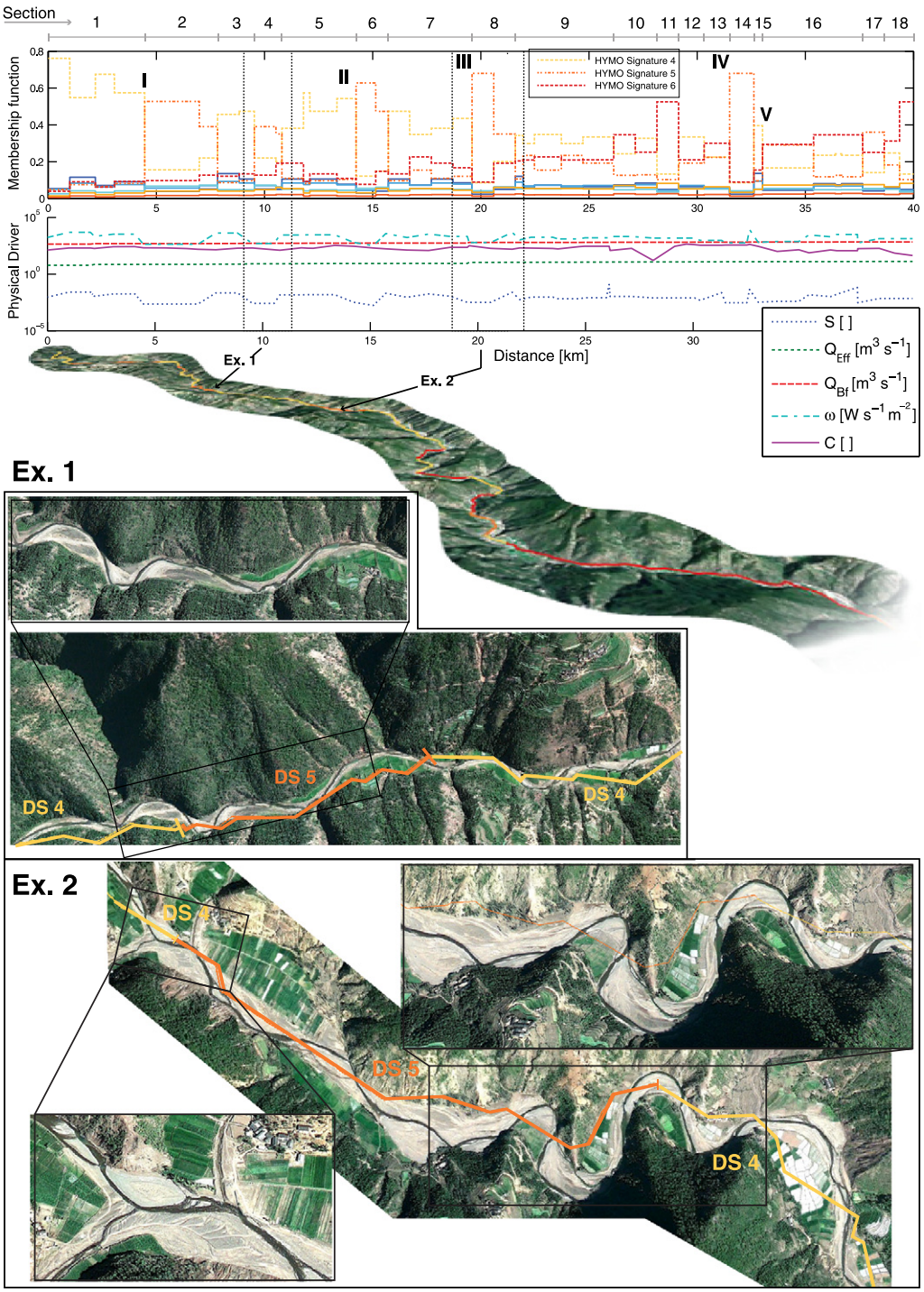

Fig. 8. Comparison of physical driver, classification results, and high resolution satellite images (Google Inc., 2013) for the validation area (Fig. 1). Sections define stretches of the river with the same dominant HYMO signature. Examples 1 and 2 are described more in detail in the text. Zoom boxes highlight key morphological features.

of fixed length ($L_{sect} = const$). $L_{sect} = 4$ was selected, similar to the average of the variable-length aggregation. The comparison with the single-section approach benchmarked in how far the model performance depended on the fact that any aggregation was applied. The fixed-section approach measured whether or not defining sections of variable length was an improvement over fixed length aggregation. For each aggregation, physical drivers as well as local values of the HYMO signatures were compared as predictors in a linear multiple regression model to predict the local response of morphological variables. From the three different aggregation approaches combined with two sets of predictors, six distinct models were constructed (Table 6).

The different models were compared using R^2 and the absolute explained variance was defined as

$$I = \frac{R^2 * \sigma^2_{aggreg}}{\sigma^2_{L_{sect}=1}} \tag{6}$$

with $\sigma^2_{aggreg.}$ being the variance in the aggregated data set and $\sigma^2_{L_{sect}=1}$ the variance in the nonaggregated data set. I took into account that the variance of the derived aggregated data sets might significantly vary amongst the different aggregation approaches. In particular, any

Table 6
Predictors and scale of analysis distinguishing the six linear multiple regression models.

	Scale of analysis	Predictor
Model 1	Variable-length sections	Physical driver
Model 2	Variable-length sections	HYMO signature
Model 3	Reach ($L_{sect} = 1$)	Physical driver
Model 4	Reach ($L_{sect} = 1$)	HYMO signature
Model 5	Fixed-length sections ($L_{sect} = 4$)	Physical driver
Model 6	Fixed-length sections ($L_{sect} = 4$)	HYMO signature

aggregation was expected to strongly reduce the variance. Thus a model based on an aggregated data set might perform very well in terms of R^2 just for the fact that the variance of input and output variables was strongly reduced. Using I as a metric, we benchmarked the models on how well they perform in reproducing the original variance (Livingstone, 2009). The higher the ratio $\sigma^2_{aggreg.}/\sigma^2_{L_{sect}=1}$ the more adequate was the aggregation in identifying river units characterized by distinctive processes and forms. The index I then assessed the models' ability to reproduce the response variables, taking into account the complexity/variability of forms (or processes) modeled.

Fig. 9 compares results of the multiple linear regression models in terms of R^2 (top) and absolute explained variance I (bottom).

Models based on the HYMO signatures as predictors and variable or fixed-length aggregation of reaches (models 2 and 6) consistently attained the highest performance in terms of R^2 for all three variables. For both aggregation approaches, the use of HYMO signatures greatly improved the model performance over using physical drivers as input variables (models 1 and 5). Nevertheless, the comparison of R^2 and I (Fig. 9, bottom), indicated that the use of R^2 was not a valid indicator

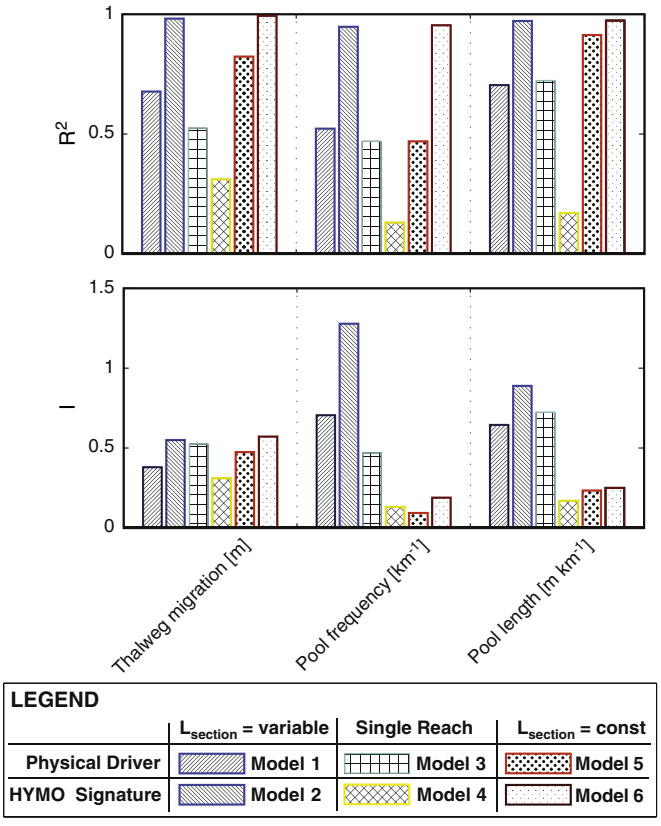

Fig. 9. Model performance in predicting morphologic variables in terms of R^2 (top panel) and explained variance I (bottom panel).

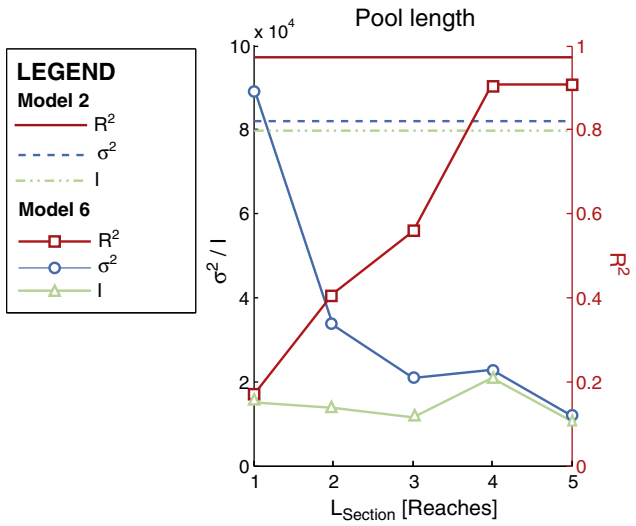

Fig. 10. Relation between variance σ^2, R^2, and explained variance I.

as it did not consider the reduction in the output variables' variance due to the aggregation procedure, and increasing R^2 due to a decrease in σ (Fig. 10). This was especially evident for pool frequency and length, for which models based on fixed length sections performed poorly. In contrast, for these variables, models based on variable section length performed well in terms of I. For thalweg migration, model performance of all models was sufficient, and model performance was more similar for the different models.

The findings indicated that: (*i*) the use of HS as predictors of local morphology outperformed the use of physical drivers; (*ii*) the proposed spatial aggregation outperformed any fixed-length spatial aggregation in terms of predictive power and absolute variance explained for morphological response variables.

6. Discussion

6.1. Potential of HYMO signatures for river characterization

Through the presented methodology we provided a framework to produce and process drivers of hydromorphology based on remote sensing data and commonly available data sets. By combining various methods of spatial analysis and classification, a consistent and scalable framework was created to characterize rivers by their geomorphological drivers especially in data-scarce environments. The approach was purely data-driven, a key requirement given the large scale of analysis, the high dimensionality of the input data set and the very limited a priori knowledge on relevant HYMO processes. Characteristic classes of reaches driven by similar physical drivers were derived without requiring an a priori definition of expected number of classes. In comparison to existing, crisp approaches (Bizzi and Lerner, 2012), the reduction of the data set into a small set of HYMO classes was not implying a loss of information due to the fuzziness of the framework, which preserved the original, physical HYMO characteristics within the HYMO signatures of each reach. The proposed scheme expanded the spatial scale of data-driven, quantitative river classification and spatial disaggregation from the scale of individual river sections (Alber and Piégay, 2011; Bizzi and Lerner, 2012) to the fluvial network of a major drainage basin while retaining high resolution information for small scale analyses of morphologic processes. On the large scale, the classification, combined with the SOM and suitable mapping, allowed for numerical as well as visual assessment of HYMO characteristics of extended landscape units which represented different hydrogeologic and topographic conditions resulting in distinct drainage network

patterns and river channel characteristics. On the smaller scale, the classification supported the geomorphological interpretation of satellite imagery and coincided with visually detectable continuous and abrupt changes. The application of dominant HYMO signatures to identify homogenous reaches along the downstream river continuum contributes to current efforts in this regard (Alber and Piégay, 2011; Leviandier et al., 2012). The HYMO signatures reflected a collection of reaches and not only represented local conditions but also epitomized an entity of reaches characterized by similar signatures. In these terms, the local HYMO signature was interpreted as an aggregation of spatially remote but physically similar reaches from the entire data set. This implied that increasing the scale of analysis, by contextualizing HYMO variables within a larger, e.g., catchment or basin, spatial context enhanced the interpretation of local geomorphological processes and forms. Combining spatial disaggregation and basin scale classification increased the quality of numerical models for small scale morphological processes. Much additional work is going to be needed to provide a physical interpretation of HYMO signatures over all presented scales of analysis. Future efforts are going to analyze the relationships between HYMO signatures and specific channel processes, forms and its resilience to external forcing — a task to which this paper only provided the initial impulse. However, HYMO signatures exemplified the potential offered by analyzing continuous, multivariate information over the river continuum of large drainage systems, a relatively recent capability that is going to change our way of analyzing and understanding rivers (Fonstad and Marcus, 2010; Carbonneau et al., 2012).

6.2. Generalization, limits and future applicability

The set of physical drivers used in this case study should be considered neither exclusive nor exhaustive. Based on readily available data sets an initial, process-related classification was derived. Considering the required data and their availability, such an initial classification can be derived for most settings world-wide. Applications range from supporting large-scale management for integrated basin management decisions to local infrastructure or water resource development for individual minor catchments.

There are several sources of uncertainties in the calculation of these HYMO drivers, especially for slope and stream power, that are due to data resolution limits and generalization issues. Channel gradient requires caution in its calculation from a DEM especially for shallow slopes (Lane and Chandler, 2003). An error was also introduced, where filling of the DEM was required and where accordingly topographic information is lost. Here, new, high resolution (e.g., 5 m), high accuracy DEMs can potentially improve the precision of slope and stream power calculations (Biron et al., 2013). Bankfull width was derived from an empirical relationship derived by remote sensing observations. However, bankfull estimates from field data showed high variability (Orr and Walsh, 2007). More recently, continuous estimates of floodplain and bankfull width have been obtained by processing remote-sensing data (Pavelsky and Smith, 2008; Johansen et al., 2011) creating novel opportunities to derive and analyze these parameters also at catchment scale (Fisher et al., 2013; Notebaert and Piégay, 2013). Hydrologic analysis is to be improved over the implemented, simplifying discharge area relation by applying physically-based hydrological models nowadays available at catchment scales (Barker et al., 2009). Thereby, also other discharge metrics, such as more extreme discharge events which strongly impact channel sediment transport processes could be included (Mount et al., 2013), enhancing our capability to assess erosion and deposition patterns on a river network scale.

The methodology was partly validated in terms of accordance with high-resolution satellite imagery using the best data available for the scale of application, however future applications might enhance the quality of the characterization using higher resolution DEMs nowadays available in many countries and calibrating ad hoc regional hydrological models. Moreover the method focused mainly on driving forces and did not include an assessment of sediment supplies, a limitation that should be addressed in future applications. So far, identification and evaluation of sediment availability and connectivity resource intensive fieldwork, and spatial analysis offer a potential alternative, here (Reinfelds et al., 2004). Future investigation has to be directed towards validating the ability of the HYMO data sets produced to characterize fluvial processes and forms. Such an investigation is going to be based on more extensive fluvial audits and field data on specific reaches and in different geographic contexts. However, the potential of the methodology to provide river managers (and, more in general, all stakeholders involved in water resource management) with a flexible yet consistent, process-related HYMO characterization for large fluvial systems, is noticeable: Such information is going to allow for a straightforward impact assessment or scenario analysis of, e.g., large-scale land use trends or climatic changes, as it allowed for the aggregation of multivariate reach characteristics and related potential for morphologic change in extended spatial entities. This analysis was enriched by the spatially explicit visualization and assessment of classification results in a suitable GIS framework. Based on this information, expensive and resource demanding field reconnaissance missions or the set-up of monitoring networks can be planned in a more cost effective way based on an a-priori classification capable of detecting abrupt changes as well as the continuity in fluvial processes. Experts or stakeholders can be easily involved in such HYMO assessments using online GIS services in a crowd mapping fashion, as demonstrated by the online resources (.kml files) enclosed with this article. Such crowed-based approaches were, e.g., applied to map impoundments in the Mekong Basin (Clayton, 2013) and could be greatly enriched including structured HYMO information, so providing a smart loop where a top-down approach (remote-sensing based) is enriched through a bottom-up one (based on field campaigns, higher precision remote sensing information — and stakeholder and expert involvement in evaluating these data) and vice versa.

River HYMO signatures based on the fuzzy membership function have shown potential to predict thalweg migration, pool frequency and length. Such a process-based predictive framework is going pioneer, for example, a more holistic view on distributed fluvial risks beyond hydrologic (e.g., flooding) but also including morphologic risk factors such as incision and deposition, lateral erosion or channel avulsion (Gilvear, 1999; Arnaud-Fassetta et al., 2009). Accordingly, it can finally result in a truly generic hydromorphological assessment that can be further enriched including spatial (e.g., land use or geologic), ecological and historical information (Bertrand et al., 2013).

Data-driven models have been successfully applied to a variety of sciences where the relatively recent increase in data storage and processing capacities led to the availability of complex, global data sets, e.g., in economics or epidemiology (Vespignani, 2009). Nowadays, such data sets are increasingly available also in environmental and geosciences (Marcus and Fonstad, 2010). In these terms, tools in fluvial geomorphology evolve towards the combination of more traditional field-based knowledge, yet a necessity to develop our understanding of any natural system, with the processing and analyzing of novel big—environmental—data that provide unprecedented power of analysis (Carbonneau et al., 2012; Notebaert and Piégay, 2013). Successful attempts have been directed towards the application of these data sets in fluvial geomorphology (Fonstad and Marcus, 2010; Alber and Piégay, 2011; Bizzi and Lerner, 2012) and the presented methodology showed the promising potential of implementing advanced, data-driven methodologies to characterize HYMO on large river systems in data-scarce environments. In the near future, such tools are going to support the development of more 'quantitative', process-based frameworks as improvement over current, rather descriptive approaches (Buffington and Montgomery, 2013). Hereby, these new tools are

going to enhance our ability to 'read the landscape' (Brierley et al., 2013), by abandoning reductionist strategies that aim to classify rivers into crisp categories, in favor of unique, location specific typologies.

7. Conclusion

A novel framework was deployed to analyze hydromorphological drivers of large fluvial systems in poorly monitored basins. The framework was based on a multivariate, fuzzy classifier. It made use of remote sensing data and few, basic hydrologic observations. Such a framework is to bridge the current gap between the conceptual understanding, the increasing scale and scope of river management efforts, and the currently available tools for assessing river hydromorphology.

Relevant hydromorphological drivers originated from freely available data sets, applying common spatial analysis techniques. Some drivers, for which only point measurements were available, were upscaled applying well tested regression techniques. For sedimentology, where no direct observations were available, a Monte-Carlo approach was implemented to derive a consistent indicator for sediment transport processes.

The so-obtained, six-dimensional data-set served as input to a two-stage, fuzzy clustering approach. The complexity of the initial data set was transferred into a low number of characteristic signatures of hydromorphological drivers. The characteristic signatures greatly enhanced the accessibility of the data set. The fuzzy approach ensures, in turn, that the original complexity in the data set is maintained and continuous as well as abrupt changes in hydro-morphology can be depicted using the derived classification.

We applied the classification over various spatial scales and also on the temporal domain to analyze and model river hydromorphology in the Red River Basin, a major basin in northern Vietnam. On the large scale, differences in topography and hydro-meteorological forces between large subbasins became evident from the aggregated signatures of their respective fluvial network. On the scale of river segments, we first demonstrated the spatial complexity and large variance in the multivariate process-rates, which manifested as a pattern of continuous and abrupt downstream change. Second, we applied the classification to analyze high resolution satellite imagery. The combination of visual analysis and the structured, hydromorphological data set enabled interpretation of the observed morphology as a result of specific, local configuration of internal and external forcings. Moreover, the numerical modelling of morphological forms and processes was greatly improved by a flexible modelling approach developed from the fuzzy signatures.

The proposed framework is going to enrich integrated water resources management by a hydromorphological assessment tool appropriate for the wide ranges of scales that are commonly acknowledged as relevant, but rarely analyzed in a consistent, state-of-the-art approach. Future work is, on the one hand, going to focus on increasing the quality of input data and a more detailed validation. On the other hand, a dynamic classifier is going to be derived to analyze future dynamics, both in terms of distributed (e.g., climate and land use change) and local, anthropogenic alterations (e.g., hydropower development). Being flexible, expandable and based on a consistent machine learning approach the framework is to contribute to fluvial science and management in general, where such integrated assessments of fluvial hydromorphology are increasingly becoming the focus of regulatory as well as scientific efforts.

Acknowledgment

We thank Prof. Dr. P. Burlando (ETH Zurich) for his advice during the development of the presented methodology. We also acknowledge the two anonymous reviewers whose comments helped to improve this paper significantly as well as the editor, Prof. Dr. R. Marston, for the consideration of this paper. This research was executed under the project IMRR (Integrated and sustainable water Management of Red–Thai Binh Rivers System in changing climate), funded by the Italian Ministry of Foreign Affairs (Delibera n. 142 del 8 Novembre 2010).

Appendix A. Supplementary data

Supplementary data associated with this article can be found in the online version. These data include .kml files for use in e.g. Google Maps of the area covering the validation case study.

References

Alber, A., Piégay, H., 2011. Spatial disaggregation and aggregation procedures for characterizing fluvial features at the network-scale: application to the Rhône basin (France). Geomorphology 125, 343–360.
Arnaud-Fassetta, G., Astrade, L., Bardou, E., Corbonnois, J., Delahaye, D., Fort, M., Gautier, E., Jacob, N., Peiry, J.L., Piégay, H., 2009. Fluvial geomorphology and flood-risk management. Géomorphologie: Revue du Groupe Français de Géomorphologie 109–128.
Asselman, N., 2000. Fitting and interpretation of sediment rating curves. J. Hydrol. 234, 228–248.
Barbour, M.T., Gerritsen, J., Snyder, B.D., Stribling, J.B., 1999. Rapid bioassessment protocols for use in streams and wadeable rivers: periphyton, benthic macroinvertebrates, and fish, Technical Report. EPA 841-B-99-002, 2nd ed. U.S. Environmental Protection Agency, Office of Water, Washington, DC, p. 20460.
Barker, D.M., Lawler, D.M., Knight, D.W., Morris, D.G., Davies, H.N., Stewart, E.J., 2009. Longitudinal distributions of river flood power: the combined automated flood, elevation and stream power (CAFES) methodology. Earth Surf. Process. Landf. 34, 280–290.
Bertrand, M., Piégay, H., Pont, D., Liébault, F., Sauquet, E., 2013. Sensitivity analysis of environmental changes associated with riverscape evolutions following sediment reintroduction: geomatic approach on the Drôme River network, France. Int. J. River Basin Manag. 11, 19–32.
Bezdek, J., 1981. Pattern Recognition with Fuzzy Objective Function Algorithms. Kluwer Academic Publishers, Norwell, MA.
Bezdek, J.C., Hathaway, R.J., Sabin, M.J., Tucker, W.T., 1987. Convergence theory for fuzzy c-means: counterexamples and repairs. IEEE Trans. Syst. Man Cybern. 17, 873–877.
Biron, P.M., Choné, G., Buffin-Bélanger, T., Demers, S., Olsen, T., 2013. Improvement of streams hydro-geomorphological assessment using LiDAR DEMs. Earth Surf. Process. Landf. 38, 1808–1821.
Bizzi, S., Lerner, D.N., 2012. Characterizing physical habitats in rivers using map-derived drivers of fluvial geomorphic processes. Geomorphology 169–170, 64–73.
Bizzi, S., Lerner, D.N., 2013. The use of stream power as an indicator of channel sensitivity to erosion and deposition processes. River Res. Appl.. http://dx.doi.org/10.1002/rra.2717 (in press).
Boon, P.J., Calow, P., Petts, G.E., 2012. River Conservation and Management. Wiley-Blackwell, Chichester, UK.
Brierley, G., Fryirs, K., Cullum, C., Tadaki, M., Huang, H.Q., Blue, B., 2013. Reading the landscape: integrating the theory and practice of geomorphology to develop place-based understandings of river systems. Prog. Phys. Geogr. 37, 601–621.
Brierley, G., Fryirs, K., Outhet, D., Massey, C., 2002. Application of the river styles framework as a basis for river management in New South Wales, Australia. Appl. Geogr. 22, 91–122.
Brierley, G.J., Fryirs, K.A., 2008. River futures: An Integrative Scientific Approach to River Repair. Island Press, Washington, DC, USA.
Buffington, J., Montgomery, D.R., 2013. Geomorphic classification of rivers. In: Shroder, J.F., Wohl, E. (Eds.), Treatise on Geomorphology. Academic Press, San Diego, CA, pp. 730–767.
Carbonneau, P., Fonstad, M.A., Marcus, W.A., Dugdale, S.J., 2012. Making riverscapes real. Geomorphology 137, 74–86.
Carbonneau, P., Piégay, H., 2012. Introduction: the growing use of imagery in fundamental and applied river sciences. In: Carbonneau, P., Piégay, H. (Eds.), Fluvial Remote Sensing for Science and Management. John Wiley & Sons, Ltd, Chichester, UK, pp. 1–17 (chapter 1).
Castelletti, A., Pianosi, F., Quach, X., Soncini-Sessa, R., 2012. Assessing water reservoirs management and development in Northern Vietnam. Hydrol. Earth Syst. Sci. 16, 189–199.
Chiu, S.L., 1994. Fuzzy model identification based on cluster estimation. J. Intell. Fuzzy Syst. 2, 267–278.
Clayton, T., 2013. It could be citizen science part 2: crowdmapping CPWF's map of hydroelectric dams in the Mekong. Online: http://mekong.waterandfood.org/archives/4271.
Dai, S., Lu, X., 2014. Sediment load change in the Yangtze River (Changjiang): a review. Geomorphology. http://dx.doi.org/10.1016/j.geomorph.2013.05.027 (in press).
Dang, T.H., Coynel, A., Orange, D., Blanc, G., Etcheber, H., Le, L.A., 2010. Long-term monitoring (1960–2008) of the river-sediment transport in the Red River Watershed (Vietnam): temporal variability and dam-reservoir impact. Sci. Total Environ. 408, 4654–4664.
Ferguson, R., 1987. Hydraulic and Sedimentary Controls of Channel Pattern. Blackwell, Oxford, UK 129–158.
Fisher, G.B., Bookhagen, B., Amos, C.B., 2013. Channel planform geometry and slopes from freely available high-spatial resolution imagery and DEM fusion: implications for channel width scalings, erosion proxies, and fluvial signatures in tectonically active landscapes. Geomorphology 194, 46–56.

Fonstad, M.A., Marcus, W.A., 2010. High resolution, basin extent observations and implications for understanding river form and process. Earth Surf. Process. Landf. 35, 680–698.

Frissell, C., Liss, W., Warren, C., Hurley, M., 1986. A hierarchical framework for stream habitat classification: viewing streams in a watershed context. Environ. Manag. 10, 199–214.

Fujisada, H., Urai, M., Iwasaki, A., 2012. Technical methodology for ASTER global DEM. IEEE Trans. Geosci. Remote Sens. 50, 3725–3736.

Garcia, M.H., 2008. Sedimentation Engineering: Processes, Management, Modeling, and Practice. American Society of Civil Engineers, Reston, VA.

Gilvear, D.J., 1999. Fluvial geomorphology and river engineering: future roles utilizing a fluvial hydrosystems framework. Geomorphology 31, 229–245.

Google Inc., 2013. Google Earth 7.0.3.8542 (Mountain View, CA).

Gupta, H., Kao, S.J., Dai, M., 2012. The role of mega dams in reducing sediment fluxes: a case study of large Asian rivers. J. Hydrol. 464–465, 447–458.

Gurnell, A., Petts, G., 2011. Hydrology and ecology of river systems. In: Peter, W. (Ed.), Treatise on Water Science. Academic Press, Oxford, UK, pp. 237–269.

Hickin, E.J., Nanson, G.C., 1984. Lateral migration rates of river bends. J. Hydraul. Eng. 110, 1557–1567.

Huang, H.Q., Nanson, G.C., 2002. A stability criterion inherent in laws governing alluvial channel flow. Earth Surf. Process. Landf. 27, 929–944.

Johansen, K., Tiede, D., Blaschke, T., Arroyo, L.A., Phinn, S., 2011. Automatic geographic object based mapping of streambed and riparian zone extent from LiDAR data in a temperate rural urban environment, Australia. Remote Sens. 3, 1139–1156.

Knighton, A.D., 1999. Downstream variation in stream power. Geomorphology 29, 293–306.

Knighton, D., 1998. Fluvial Forms and Processes: A New Perspective, 2nd ed. Arnold, London.

Kohonen, T., 1990. The self-organizing map. Proc. IEEE 78, 1464–1480.

Kondolf, G.M., Montgomery, D.R., Piégay, H., Schmitt, L., 2003. Geomorphic classification of rivers and streams. In: Kondolf, G.M., Piégay, H. (Eds.), Tools in Fluvial Geomorphology. J. Wiley and Sons, Chichester, UK, pp. 169–202.

Lall, U., 2011. "Developing" hydrology or hydromorphology: a modern research agenda that can inform the trenches. AGU Fall Meeting Abstracts.

Lane, S.N., Chandler, J.H., 2003. Editorial: the generation of high quality topographic data for hydrology and geomorphology: new data sources, new applications and new problems. Earth Surface Processes and Landforms, John Wiley & Sons, Ltd. 28, 229–230.

Le, T.P.Q., Garnier, J., Gilles, B., Sylvain, T., Van Minh, C., 2007. The changing flow regime and sediment load of the Red River, Viet Nam. J. Hydrol. 334, 199–214.

Leviandier, T., Alber, A., Le Ber, F., Piégay, H., 2012. Comparison of statistical algorithms for detecting homogeneous river reaches along a longitudinal continuum. Geomorphology 138, 130–144.

Livingstone, D.J., 2009. A Practical Guide to Scientific Data Analysis. Wiley, Chichester, UK.

Lu, X.X., Siew, R.Y., 2006. Water discharge and sediment flux changes over the past decades in the lower Mekong river: possible impacts of the Chinese dams. Hydrol. Earth Syst. Sci. 10, 181–195.

Marcus, W.A., Fonstad, M.A., 2008. Optical remote mapping of rivers at sub-meter resolutions and watershed extents. Earth Surf. Process. Landf. 33, 4–24.

Marcus, W.A., Fonstad, M.A., 2010. Remote sensing of rivers: the emergence of a subdiscipline in the river sciences. Earth Surf. Process. Landf. 35, 1867–1872.

Meyer-Peter, E., Müller, R., 1948. Formulas for bed-load transport. Proceedings of the 2nd Meeting of the International Association for Hydraulic Structures Research. International Association of Hydraulic Research Delft., pp. 39–64.

Mount, N.J., Tate, N.J., Sarker, M.H., Thorne, C.R., 2013. Evolutionary, multi-scale analysis of river bank line retreat using continuous wavelet transforms: Jamuna River, Bangladesh. Geomorphology 183, 82–95.

Nanson, G.C., Hickin, E.J., 1986. A statistical analysis of bank erosion and channel migration in Western Canada. Geol. Soc. Am. Bull. 97, 497–504.

Nardi, F., Vivoni, E.R., Grimaldi, S., 2006. Investigating a floodplain scaling relation using a hydrogeomorphic delineation method. Water Resour. Res. 42, W09409.

Negrel, J., Kosuth, P., Bercher, N., 2011. Estimating river discharge from earth observation measurement of river surface hydraulic variables. Hydrol. Earth Syst. Sci. 15, 2049–2058.

Newson, M.D., Large, A.R.G., 2006. 'Natural' rivers, 'hydromorphological quality' and river restoration: a challenging new agenda for applied fluvial geomorphology. Earth Surf. Process. Landf. 31, 1606–1624.

Nicoll, T.J., Hickin, E.J., 2010. Planform geometry and channel migration of confined meandering rivers on the Canadian prairies. Geomorphology 116, 37–47.

Notebaert, B., Piégay, H., 2013. Multi-scale factors controlling the pattern of floodplain width at a network scale: The case of the Rhône basin, France. Geomorphology 200, 155–171.

O'Callaghan, J.F., Mark, D.M., 1984. The extraction of drainage networks from digital elevation data. Comp. Vision Graph. Image Process. 28, 323–344.

Orr, H.G., Large, A.R.G., Newson, M.D., Walsh, C.L., 2008. A predictive typology for characterising hydromorphology. Geomorphology 100, 32–40.

Orr, H.G., Walsh, C.L., 2007. Incorporating Climate Change in River Typologies: Results. Technical Report. Environment Agency, Bristol, UK.

Parsons, M., Thoms, C.M., Norris, R.H., 2003. Development of a standardised approach to river habitat assessment in Australia. Environ. Monit. Assess. 98, 109–130.

Pavelsky, T.M., Smith, L.C., 2008. RivWidth: a software tool for the calculation of river widths from remotely sensed imagery. IEEE Geosci. Remote Sens. Lett. 5, 70–73.

Petts, G.E., Amoros, C., 1996. Fluvial Hydrosystems. Chapman & Hall, London, UK.

Poole, G.C., 2002. Fluvial landscape ecology: addressing uniqueness within the river discontinuum. Freshw. Biol. 47, 641–660.

Rangin, C., Klein, M., Roques, D., Le Pichon, X., Van Trong, L., 1995. The Red River fault system in the Tonkin Gulf, Vietnam. Tectonophysics 243, 209–222.

Raven, P.J., Holmes, N., Dawson, F.H., Everard, M., 1998. Quality assessment using River Habitat Survey data. Aquat. Conserv. Mar. Freshw. Ecosyst. 8, 477–499.

Reinfelds, I., Cohen, T., Batten, P., Brierley, G., 2004. Assessment of downstream trends in channel gradient, total and specific stream power: a GIS approach. Geomorphology 60, 403–416.

Richards, K., Brasington, J., Hughes, F., 2002. Geomorphic dynamics of floodplains: ecological implications and a potential modelling strategy. Freshw. Biol. 47, 559–579.

Rieger, W., 1993. Automated river line and catchment area extraction from DEM data. Int. Arch. Photogramm. Remote. Sens. 29, 642–649.

Rieger, W., 1998. A phenomenon-based approach to upslope contributing area and depressions in DEMs. Hydrol. Process. 12, 857–872.

Rinaldi, M., Surian, N., Comiti, F., Bussettini, M., 2013. A method for the assessment and analysis of the hydromorphological condition of Italian streams: the Morphological Quality Index (MQI). Geomorphology 180–181, 96–108.

Saito, Y., Chaimanee, N., Jarupongsakul, T., Syvitski, J.P., 2007. Shrinking megadeltas in Asia: sea-level rise and sediment reduction impacts from case study of the Chao Phraya delta. Inprint Newsletter of the IGBP/IHDP Land Ocean Interaction in the Coastal Zone 2, pp. 3–9.

Sear, D.A., Newson, M.D., Thorne, C.R., 2010. Guidebook of Applied Fluvial Geomorphology. Thomas Telford, London, UK.

Simon, A., Doyle, M., Kondolf, G.M., Shields, F.D.J., Rhoads, B., McPhillips, M., 2007. Critical evaluation of how the Rosgen classification and associated natural channel design methods fail to integrate and quantify fluvial processes and channel response. J. Am. Water Res. Assoc. 43, 1117–1131.

Simon, A., Rinaldi, M., 2006. Disturbance, stream incision, and channel evolution: the roles of excess transport capacity and boundary materials in controlling channel response. Geomorphology 79, 361–383.

Somerville, D., Pruitt, B.A., 2004. A Review of Selected Protocols for Use in the Clean Water Act Section 404 Program. Technical Report. U.S. Environmental Protection Agency, Office of Wetlands, Oceans, and Watersheds, Wetlands Division, Washington, DC.

Strahler, A.N., 1957. Quantitative analysis of watershed geomorphology. Trans. Am. Geophys. Union 38, 913–920.

Syvitski, J.P., Kettner, A.J., Overeem, I., Hutton, E.W., Hannon, M.T., Brakenridge, G.R., Day, J., Vörösmarty, C., Saito, Y., Giosan, L., et al., 2009. Sinking deltas due to human activities. Nat. Geosci. 2, 681–686.

Thanh, T., Saito, Y., Huy, D., Nguyen, V., Ta, T., Tateishi, M., 2004. Regimes of human and climate impacts on coastal changes in Vietnam. Reg. Environ. Chang. 4, 49–62.

Thorp, J.H., Thoms, M.C., Delong, M.D., 2006. The riverine ecosystem synthesis: biocomplexity in river and networks across space and time. River Res. Appl. 22, 123–147.

Trinh, P.T., Van Liem, N., Van Huong, N., Vinh, H.Q., Van Thom, B., Thao, B.T., Tan, M.T., Hoang, N., 2012. Late Quaternary tectonics and seismotectonics along the Red River fault zone, North Vietnam. Earth Sci. Rev. 114, 224–235.

Van Maren, D., 2005. Barrier formation on an actively prograding delta system: the Red River Delta, Vietnam. Mar. Geol. 224, 123–143.

Vannote, R.L., Minshall, G.W., Cummins, K.W., Sedell, J.R., Cushing, C.E., 1980. The river continuum concept. Can. J. Fish. Aquat. Sci. 37, 130–137.

Vaughan, I.P., Diamond, M., Gurnell, A.M., Hall, K.A., Jenkins, A., Milner, N.J., Naylor, L.A., Sear, D.A., Woodward, G., Ormerod, S.J., 2009. Integrating ecology with hydromorphology: a priority for river science and management. Aquat. Conserv. Mar. Freshw. Ecosyst. 19, 113–125.

Vaughan, I.P., Ormerod, S.J., 2010. Linking ecological and hydromorphological data: approaches, challenges and future prospects for riverine science. Aquat. Conserv. Mar. Freshwat. Ecosyst. 20, S125–S130.

Vespignani, A., 2009. Predicting the behavior of techno-social systems. Science 325, 425–428.

Vocal Ferencevic, M., Ashmore, P., 2012. Creating and evaluating digital elevation model-based stream-power map as a stream assessment tool. River Res. Appl. 28, 1394–1416.

Walling, D., Fang, D., 2003. Recent trends in the suspended sediment loads of the world's rivers. Glob. Planet. Chang. 39, 111–126.

Whigham, P.A., Young, W.J., 2001. Modelling river and floodplain interactions for ecological response. Math. Comput. Model. 33, 635–647.

Wohl, E., 2006. Human impacts to mountain streams. Geomorphology 79, 217–248.

Wolman, M.G., Miller, J.P., 1960. Magnitude and frequency of forces in geomorphic processes. J. Geol. 68, 54–74.

Wong, M., Parker, G., 2006. Reanalysis and correction of bed-load relation of Meyer-Peter and Müller using their own database. J. Hydraul. Eng. 132, 1159–1168.

Yager, R.R., Fileu, D.P., 1993. Learning of fuzzy rules by mountain clustering. In: Bosacchi, B., Bezdek, J.C. (Eds.), Applications of Fuzzy Logic Technology. International Society for Optics and Photonics, Boston, MA, pp. 246–254.

Yang, Z., Wang, H., Saito, Y., Milliman, J.D., Xu, K., Qiao, S., Shi, G., 2006. Dam impacts on the Changjiang (Yangtze) River sediment discharge to the sea: the past 55 years and after the Three Gorges Dam. Water Resour. Res. 42.